COMMUNICATION

Check for updates

Anisotropy control in magnetic nanostructures through field-assisted chemical vapor deposition†

Daniel Stadler, [ID] [a] Thomas Brede, [ID] [b] Danny Schwarzbach,[b] Fernando Maccari, [ID] [c] Thomas Fischer, [ID] [a] Oliver Gutfleisch, [ID] [c] Cynthia A. Volkert[b] and Sanjay Mathur [ID] *[a]

Chemical vapor deposition of iron pentacarbonyl (Fe(CO)$_5$) in an external magnetic field ($B = 1.00$ T) was found to significantly affect the microstructure and anisotropy of as-deposited iron crystallites that could be transformed into anisotropic hematite (α-Fe$_2$O$_3$) nanorods by aerobic oxidation. The deterministic influence of external magnetic fields on CVD deposits was found to be substrate-independent as demonstrated by the growth of anisotropic α-Fe columns on FTO (F:SnO$_2$) and Si (100), whereas the films deposited in the absence of the magnetic field were constituted by isotropic grains. TEM images revealed gradual increase in average crystallite size in correlation to the increasing field strength and orientation, which indicates the potential of magnetic field-assisted chemical vapor deposition (mfCVD) in controlling the texture of the CVD grown thin films. Given the facet-dependent activity of hematite in forming surface-oxygenated intermediates, exposure of crystalline facets and planes with high atomic density and electron mobilities is crucial for oxygen evolution reactions. The field-induced anisotropy in iron nanocolumns acting as templates for growing textured hematite pillars resulted in two-fold higher photoelectrochemical efficiency for hematite films grown under external magnetic fields ($J = 0.050$ mA cm^{-2}), when compared to films grown in zero field ($J = 0.027$ mA cm^{-2}). The dark current measurements indicated faster surface kinetics as the origin of the increased catalytic activity.

Introduction

Iron, a classical ferromagnet (2.22 μ_B), is an excellent candidate for investigating the effect of external magnetic field on metallic iron films grown below its Curie temperature (770 °C) by chemical vapor deposition (CVD).[1] A large body of data is available on the formation of iron films on silicon[2–4] or platinum[5] using iron pentacarbonyl (Fe(CO)$_5$) as molecular precursor, however, so far a direct influence of external magnetic field during CVD film growth has not been examined. Specifically, the microstructure evolution during the CVD process is challenging to manipulate by external stimuli and the experimental strategies are mostly limited to external orientation-aids, such as pre-structured surfaces,[6,7] templates[8] or external magnetic fields.[9] Kim and coworkers observed an anisotropic assembly of iron clusters during magnetic field-assisted hot filament CVD,[10,11] when iron nanoclusters formed in the gas phase were found to align on the substrate along the magnetic field lines. Luo *et al.* applied magnetic fields during the growth of carbon nanotubes (CNTs) on nickel catalyst to demonstrate growth parallel to the field direction and elongation of catalyst particles that consequently favored the CNT growth in the direction of the applied field.[9] Similarly, application of magnetic fields was shown to promote crystal growth during CVD of diamond films.[12,13] Recently, Wang *et al.* reported on the magnetic and electrical field effects in the CVD of diamond films, when thinner coatings with preferred orientation were obtained during the field-assisted processes.[12]

The interaction of magnetic materials with an externally applied magnetic field strongly depends on structure, size, temperature and magnetic characteristics of the atoms, and embryonic clusters of the growing material.[1] Reports describing positive magnetic field-effects on structure evolution, crystallinity and performance of hematite thin films, as obtained from PECVD processes are promising;[14] however, literature lacks on magnetic field influences during structure formation in metal-organic CVD. In this work, we demonstrate magnetic field-assisted cold wall CVD (mfCVD) as a suitable method for the preparation of anisotropically grown iron nanostructures followed by their conversion into hematite films, examined towards their photoelectrochemical activity.

[a]Institute of Inorganic Chemistry, Department of Chemistry, University of Cologne, Greinstr. 6, D-50939 Cologne, Germany. E-mail: sanjay.mathur@uni-koeln.de

[b]Institute of Materials Physics, University of Goettingen, Friedrich-Hund-Platz 1, D-37077 Goettingen, Germany

[c]Materials Science, Technische Universität Darmstadt, Alarich-Weiss-Str. 16, D-64287 Darmstadt, Germany

Results and discussion

A customized cold wall CVD set-up built for performing film growth in external magnetic fields ($0.00 \leq B \leq 1.00$ T) was used in this study to investigate the decomposition of $Fe(CO)_5$ in mfCVD (Fig. 1). A non-metallic resistive DC heater was used to avoid perturbances in the applied magnetic field. The temperature of the precursor reservoir and substrate holder was monitored during the entire process.

Besides electric field interferences from the heater, thermal fluctuations in magnet materials can result in demagnetization events thereby leading to variations in field strength and homogeneity.[1] Since no significant heating of the magnet was observed within the time period of the deposition processes (see Fig. S1†), influence of thermally induced heat perturbations of the magnetic field can be excluded. Additionally, the time dependent stability of the applied magnetic field was measured at a field flux density of 1.00 T that confirmed stable processing conditions (Fig. S1D†). Since neither field fluctuations nor heating of the magnet were detected, the externally applied magnetic field was determined and considered as constant during all mfCVD processes.

Deposition of metallic iron films with and without an external magnetic field (1.00 T), using $Fe(CO)_5$ as the iron source, was performed at 300 °C substrate temperature. The orientation of the magnetic field with respect to the substrate was found to have significant influence on the obtained film morphologies and thus on underlying nucleation and grain growth mechanisms. For instance, a perpendicular field orientation ($\alpha = 90°$) led to anisotropic α-Fe crystallites (Fig. 2C), whereas a homogeneous coating constituted by equiaxed grains was observed for the deposition performed without an external magnetic field (Fig. 2D). When the applied field was parallel ($\alpha = 0°$) to the substrate, larger crystallites with cuboidal morphology were obtained, however a tilted orientation of anisotropic grains was evident at 45° inclination. The XRD patterns confirmed the formation of α-Fe for both field-assisted and zero field experiments (see Fig. S3†).

The CVD of α-Fe under the variation of field strength (from $0.25 \leq B \leq 1.00$ T) revealed that oriented structures were formed in all cases with better alignment at higher field strengths (Fig. 3). While homogeneous structures were observed at higher magnetic field flux density ($B = 1.00$ T), the perpendicular orientation of the iron columns was less pronounced with
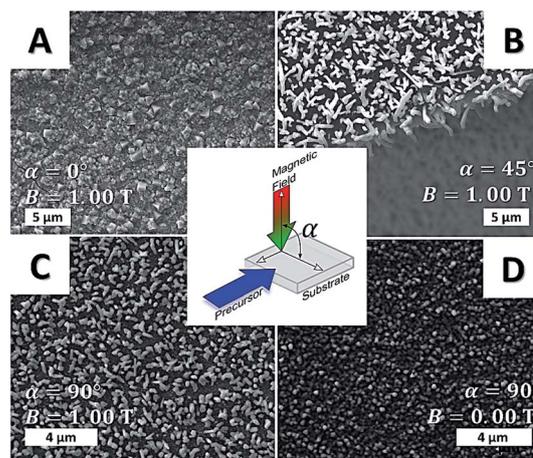

Fig. 2 SEM micrographs of iron films deposited in the presence of parallel (A), 45° (B) and orthogonal (C) applied magnetic field. The control experiment (zero field) is highlighted in (D). For experimental details, see ESI.†

decreasing field strength, as observed in the top view SEM images (Fig. 3D–F). This field dependent orientation of the anisotropic iron structures illustrated the general impact of external fields on as-grown films and their implication in tailoring the grain structure and texture in the film (see Fig. S4–S6 in ESI†).

Cross-sectional TEM images of the films grown at 1.00 T (Fig. 4A and C) and 0.25 T (Fig. 4B and D, $\alpha = 90°$) confirmed the increase in crystal size at larger magnetic fields thereby supporting the hypothesis that on-substrate nucleation and grain growth (diffusion) is strongly influenced by magnetic interactions between the crystalline nuclei and applied magnetic field. These results were also obtained in case of ReN depositions from single-source precursors[15] and diamond coatings[12] and as such in good agreement with literature results. The increase of grain size during annealing of bulk phase magnetic materials is reported, however at much higher magnetic fields (6 T).[16–18]

The results of room temperature isothermal magnetization measurements (Fig. 5A and B) present the magnetic behavior of the samples grown with applied field of 0.25 T and 0.50 T. The measurements performed in parallel direction (with respect to the field applied during film deposition) show no significant difference in their magnetic response. However, in the
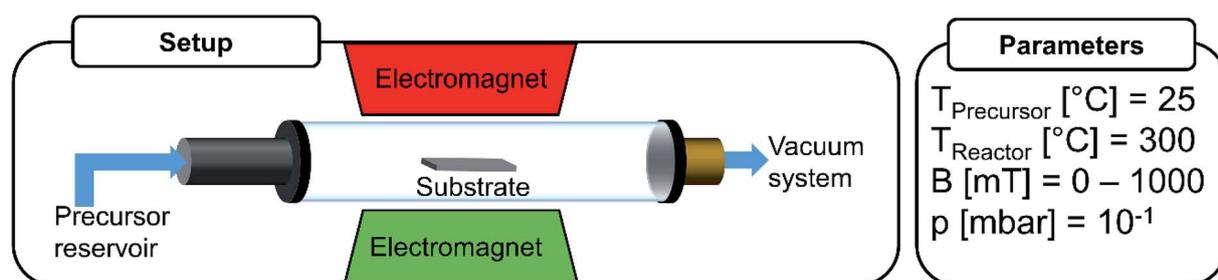

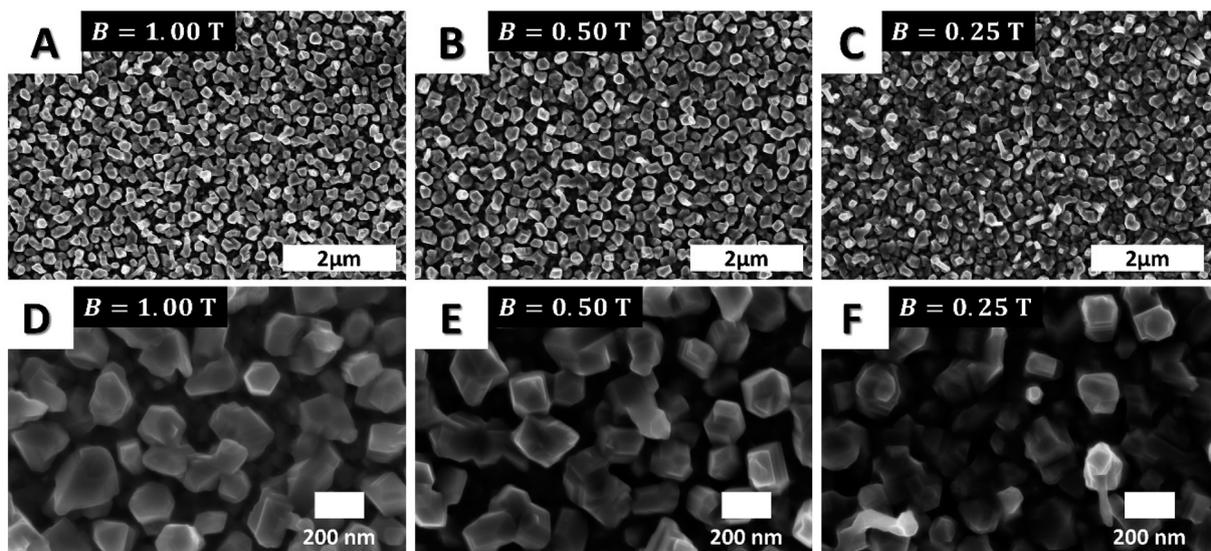Fig. 1 Schematic sketch of the CVD setup and parameters used for mfCVD experiments.

Fig. 3 SEM micrographs of the films deposited in CVD experiments performed with 1.00 T (A and D), 0.50 T (B and E) and 0.25 T (C and F) field strengths. With decreasing field flux densities, a gradual decrease in the alignment of the vertical structure was observed revealing the evident directionality of grains in mfCVD experiments. All experiments were performed with perpendicular field orientation ($\alpha = 90°$).

perpendicular measurement direction, both samples present a clear anisotropic behavior, denoted by the higher magnetic field applied in order to saturate the samples. This difference between both directions can be attributed to the magnetic shape anisotropy induced by the texture introduced during the film grown. Comparing the magnetization measurements (perpendicular direction) of both films, in combination with SEM analysis, the different behavior can be attributed to the grain size and orientation development caused by the mfCVD process. For precise quantification of shape anisotropy, more analysis are necessary which goes beyond the scope of the current work.

The influence of external magnetic fields was found to be substrate-independent as demonstrated by growth of aniso-tropic α-Fe columns on FTO (F:SnO$_2$), whereas the zero field experiment produced isotropic films (Fig. S7†). The possibility of growing anisotropic structures on various substrates opens

up new possibilities for tuning material properties without any compositional changes.

Aerobic annealing of anisotropic α-Fe columns produced elongated hematite grains (Fig. 6), whereas isotropic crystallites were observed for α-Fe samples grown in the absence of external field and annealed under similar conditions. The cross-sectional SEM studies of field-assisted and zero field samples annealed in air under similar conditions exhibited higher degree of densification of grains in field-assisted experiments, while smaller grains were visible for zero field deposition. Furthermore, microscopic structural defects (white arrows, Fig. 6) were observed for the zero field experiment (Fig. 6B), while no inhomogeneities were visible in samples grown in field-assisted process (Fig. 6D). The absence of structural inhomogeneities emphasizes a densification effect of magnetic fields on iron film formation, while zero field experiments lead to more chaotic growth. Consequently, void formation is more
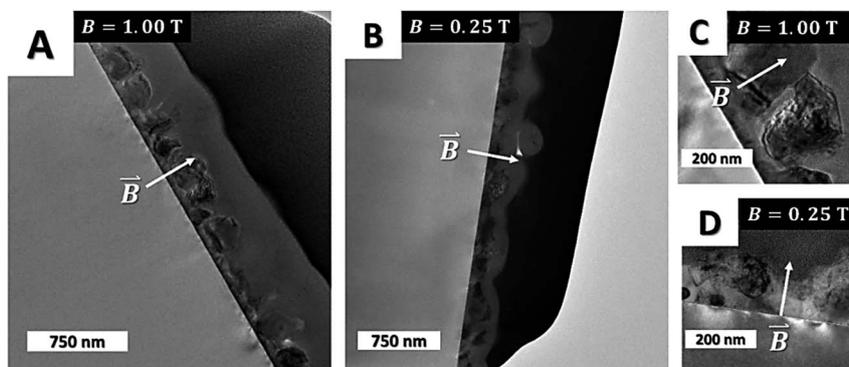

Fig. 4 Cross-sectional TEM images of iron films formed in CVD experiments carried out at 1.00 T (A and C) and 0.25 T magnetic field (B and D). Larger crystals are visible for mfCVD films deposited under higher applied magnetic field. The white arrows indicate the direction of the applied field.
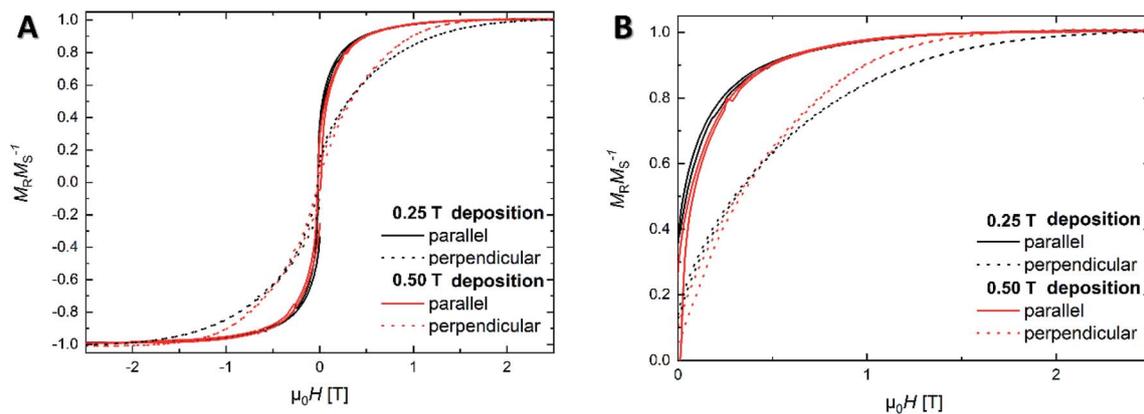
Fig. 5 (A) In-plane (solid line) and out-of-plane (dashed line) magnetic measurements of the samples grown at 0.25 T (red) and 0.50 T (black). (B) Demonstrated an increased out of plane magnetization of the sample in case of higher applied magnetic field strengths. All measurements were performed at 300 K.

likely to occur in the absence of magnetic fields, especially in case of fast growth kinetics. In contrast, the surface roughness was higher for the samples obtained *via* field-assisted CVD process, while the zero field case revealed a smooth and homogeneous surface. XRD analysis of oxidized films (Fig. 6C and F) demonstrated a significant texturing for samples grown in field-assisted deposition with predominance of diffraction planes (104), (113), (024), (116) and (018). Remarkably, no signal for (110) plane was detected, indicating a suppression of crystal growth along this direction through field-assisted deposition of anisotropic nanostructures. In contrast, no identifiable peaks were observed for zero field experiment, indicating the

formation of mainly amorphous iron oxide. Since the sample formed in field-assisted process exhibits a higher exposure to air, more oxygen gets in contact with the specimen. Therefore, an increased oxygen pressure is assumed inside the lattice of the field-assisted sample, leading to fast crystallization in contrast to the zero field sample. Thus, another striking influence of external magnetic fields seemed to promote post-processing crystallization probably due to the previously described formation of larger crystals during the mfCVD process. EDX analysis of the samples performed at 5 kV excitation voltage (Fig. S8†) revealed the presence of iron and oxygen without further impurities in the film. Due to the high
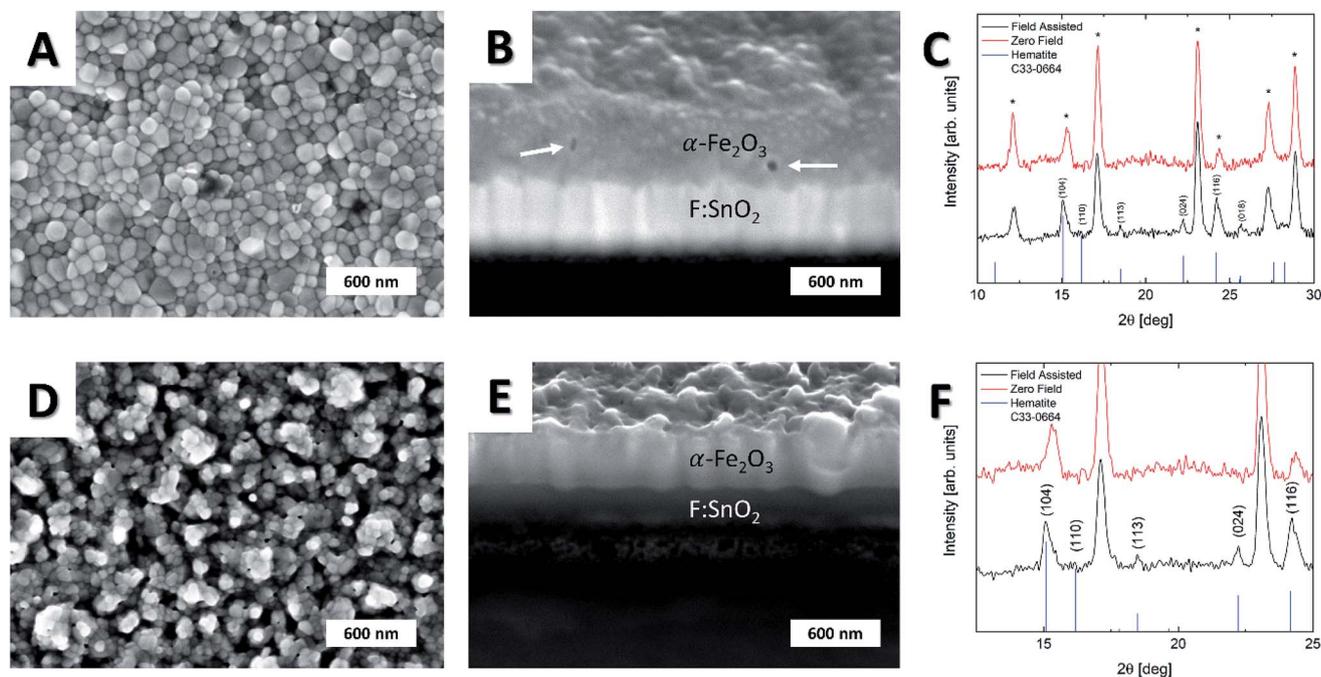

Fig. 6 SEM micrographs of hematite nanostructures on FTO after annealing of the obtained iron films from zero field (A and B) and 1.00 T (D and E) experiments. Corresponding XRD patterns are presented (C and F, detailed view) for zero field (red) and field-assisted (black, 1.00 T) experiments. Substrate peaks are marked with (*) and identified as cassiterite from pdf file C41-1445.
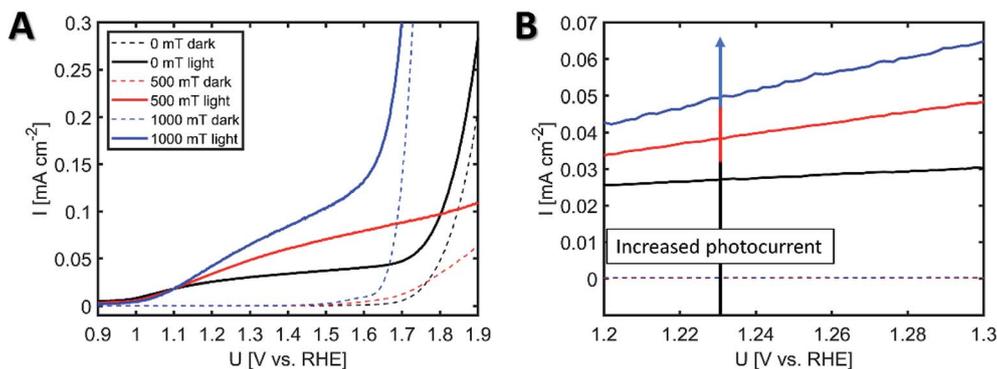
Fig. 7 (A) PEC measurements for annealed samples deposited in 0 mT (black), 500 mT (red) and 1000 mT (blue) and (B) field dependent increase in photocurrent at water splitting potential of 1.23 V (arrow).

anisotropy and small thickness of the film, a further quantification of atomistic ratio was not performable.

Hematite is a well-known photoanode material for photoelectrochemical (PEC) water-splitting reactions and especially one dimensional hematite nanoarrays are reported to exhibit improved PEC performance due to the presence of (110) planes that have higher electron mobilities[19,20] and are exposed in anisotropic hematite nanorods.[21,22] Various fabrication methods ranging from CVD of single source precursor molecules[23,24] and PECVD deposition of iron oxides[25–28] to solution processing[29,30] are known for producing hematite for conducting water-splitting reactions. The PEC activities of hematite films obtained after the thermal oxidation of iron crystals grown with (mfCVD) and without (CVD) field were analyzed in alkaline conditions and the recorded photocurrent values are presented in Fig. 7.

The hematite films obtained from the iron sample deposited at 1.00 T had a photocurrent density of $J = 0.050$ mA cm^{-2} at 1.23 V (versus reversible hydrogen electrode (RHE)), while the film obtained from zero field experiments showed lower photocurrent density of $J = 0.027$ mA cm^{-2}. The samples obtained at 0.50 T exhibited a photocurrent density of $J = 0.038$ mA cm^{-2} verifying the trend observed in the crystal orientation as a function of field strength (see Fig. 7B). Since field-assisted deposition revealed higher crystallinity (XRD evidence, Fig. 6C) and surface area compared to zero field control experiment, both better charge transport properties and higher photoelectrochemically-active surface area need to be considered when evaluating the enhanced photocurrent values of the samples grown in mfCVD. Intriguingly, the XRD diffraction peak for (110) plane responsible for the favorable facet for improving PEC kinetics[19] was found to be suppressed in field-assisted deposition, ruling out crystallographic orientation as the reason for observed PEC performances. This suggests that increased surface area and promoted reaction kinetics are apparently the dominating factors for enhanced catalytic activity, since a shifted onset in dark current measurements was observed with increasing field strengths. The lower PEC performance for zero field deposition samples can be explained by smaller grains and thus increased grain boundary density

that is known to lower PEC performance due to higher charge recombination. These observations are in good agreement with SEM and XRD data. The observed electrochemical performance for the 0.50 T deposition does not follow the same trend with respect to the electrocatalytic properties at voltages above 1.7 V. Most likely, crack and pinhole formation lead to the exposure of FTO to the alkaline solution, lowering the electrocatalytic activity of the film. Nevertheless, the observed changes in photocatalytic activity and onset potential stay in line with the presented field-related trend.

Conclusion

The effect of external magnetic fields on the chemical vapor deposition of ferromagnetic iron nanostructures revealed strong effects of external magnetic fields on the phase composition, grain growth and densification processes. A significant altering of morphology, chemical topography and functional properties of films deposited in the presence of external magnetic fields was furthermore observed. The application of an external magnetic field was found to be independent of the nature of substrate and anisotropic structures were obtained on both silicon and FTO in the mfCVD process. With decreasing field strengths, a suppressed collinear orientation with respect to the applied magnetic field was seen so that larger α-Fe crystals were obtained for field-assisted processing, while a variation of field orientation resulted in different morphologies. Annealing the substrates led to the phase-selective transformation of iron grains to hematite nanostructures with higher (field-assisted CVD) and lower (zero field CVD) aerial density of hematite nanostructures. The structural and topological differences of hematite films were found to be responsible for differential photoelectrocatalytic properties of the two sets of samples with higher photocurrent and thus higher water-splitting ability was observed for samples processed in mfCVD. In summary, magnetic field-assisted CVD offers a catalyst-free method for the anisotropic formation of iron nanostructures. This method might provide deeper insights into field – matter interactions during film formation and thus offers additional control on film morphologies. Finally, this research demonstrates that external magnetic fields can expand the

experimental space of CVD to provide an additional control parameter for influencing the characteristics of as-grown thin films.

Conflicts of interest

The authors declare no competing financial interests.

Acknowledgements

References

1 J. M. Coey, *Magnetism and Magnetic Materials*, Cambridge University Press, 2010.

2 R. Jackman and J. Foord, *Surf. Sci.*, 1989, **209**, 151–158.

3 N. Gluck, Z. Ying, C. Bartosch and W. Ho, *J. Chem. Phys.*, 1987, **86**, 4957–4978.

4 K. Rührnschopf, D. Borgmann and G. Wedler, *Thin Solid Films*, 1996, **280**, 171–177.

5 F. Zaera, *Langmuir*, 1991, **7**, 1188–1191.

6 S. Mathur, S. Barth, U. Werner, F. Hernandez-Ramirez and A. Romano-Rodriguez, *Adv. Mater.*, 2008, **20**, 1550–1554.

7 J.-J. Wu and S.-C. Liu, *J. Phys. Chem. B*, 2002, **106**, 9546–9551.

8 D. Luo, L. Wu and J. Zhi, *ACS Nano*, 2009, **3**, 2121–2128.

9 C. Luo, Q. Fu and C. Pan, *Sci. Rep.*, 2015, **5**, 9062.

10 D.-H. Kim, H.-S. Jang, H.-R. Lee, C.-D. Kim and H.-D. Kang, *Appl. Phys. Lett.*, 2004, **85**, 109–111.

11 G. H. Lee, S. H. Huh, J. W. Jeong, S. H. Kim, B. J. Choi, B. Kim and J. Park, *Scr. Mater.*, 2003, **49**, 1151–1155.

12 Y. Wang, J. Li, N. Hu, Y. Jiang, Q. Wei, Z. Yu, H. Long, H. Zhu, Y. Xie, L. Ma, C.-T. Lin and W. Su, *Mater. Res. Express*, 2018, **5**, 035009.

13 X. You, Z. Yu, L. Shi and L. Wang, *J. Cryst. Growth*, 2009, **311**, 4675–4678.

14 M. Pyeon, V. Rauch, D. Stadler, M. Gürsoy, M. Deo, Y. Gönüllü, T. Fischer, T. Hwang and S. Mathur, *Adv. Eng. Mater.*, 2019, 1900195.

15 M. Frank, L. Jürgensen, D. Stadler, D. Graf, I. Gessner, F. Zajusch, T. Fischer, M.-A. Rose, D. N. Mueller and S. Mathur, *Inorg. Chem.*, 2019, **58**, 10408–10416.

16 T. Watanabe, S. Tsurekawa, X. Zhao, L. Zuo and C. Esling, *J. Mater. Sci.*, 2006, **41**, 7747–7759.

17 S. Rivoirard, *JOM*, 2013, **65**, 901–909.

18 O. Guillon, C. Elsässer, O. Gutfleisch, J. Janek, S. Korte-Kerzel, D. Raabe and C. A. Volkert, *Mater. Today*, 2018, **5**, 527–536.

19 S. Kment, P. Schmuki, Z. Hubicka, L. Machala, R. Kirchgeorg, N. Liu, L. Wang, K. Lee, J. Olejnicek and M. Cada, *ACS Nano*, 2015, **9**, 7113–7123.

20 D. A. Grave, N. Yatom, D. S. Ellis, M. C. Toroker and A. Rothschild, *Adv. Mater.*, 2018, **30**, e1706577.

21 R. Morrish, M. Rahman, J. D. MacElroy and C. A. Wolden, *ChemSusChem*, 2011, **4**, 474–479.

22 Gurudayal, S. Y. Chiam, M. H. Kumar, P. S. Bassi, H. L. Seng, J. Barber and L. H. Wong, *ACS Appl. Mater. Interfaces*, 2014, **6**, 5852–5859.

23 J. Leduc, Y. Gönüllü, P. Ghamgosar, S. You, J. Mouzon, H. Choi, A. Vomiero, M. Grosch and S. Mathur, *ACS Appl. Nano Mater.*, 2019, **2**, 334–342.

24 S. Mathur, M. Veith, V. Sivakov, H. Shen, V. Huch, U. Hartmann and H. B. Gao, *Chem. Vap. Deposition*, 2002, **8**, 277–283.

25 D. Barreca, G. Carraro, A. Gasparotto, C. Maccato, C. Sada, A. P. Singh, S. Mathur, A. Mettenbörger, E. Bontempi and L. E. Depero, *Int. J. Hydrogen Energy*, 2013, **38**, 14189–14199.

26 A. Mettenbörger, Y. Gönüllü, T. Fischer, T. Heisig, A. Sasinska, C. Maccato, G. Carraro, C. Sada, D. Barreca and L. Mayrhofer, *Nano Energy*, 2016, **19**, 415–427.

27 A. Mettenbörger, T. Singh, A. P. Singh, T. T. Järvi, M. Moseler, M. Valldor and S. Mathur, *Int. J. Hydrogen Energy*, 2014, **39**, 4828–4835.

28 A. P. Singh, A. Mettenbörger, P. Golus and S. Mathur, *Int. J. Hydrogen Energy*, 2012, **37**, 13983–13988.

29 L. Wang, T. Nakajima and Y. Zhang, *J. Mater. Chem. A*, 2019, **7**, 5258–5265.

30 A. Y. Ahmed, M. G. Ahmed and T. A. Kandiel, *Appl. Catal., B*, 2018, **236**, 117–124.